Available online at www.sciencedirect.com
ScienceDirect
Trans. Nonferrous Met. Soc. China 33(2023) 958−968
Transactions of Nonferrous Metals Society of China
www.tnmsc.cn

Numerical simulation and multi-objective parameter optimization of gas−liquid flow in horizontal stirred tank

Liu LIU[1], Zhi-bin CHEN[1], Hong-jie YAN[1], Deng-kai ZHANG[2], Ping ZHOU[1]

1. School of Energy Science and Engineering, Central South University, Changsha 410083, China;
2. Danxia Smelter, Shenzhen Zhongjin Lingnan Non-ferrous Metal Company Limited, Shaoguan 512325, China

Received 4 January 2022; accepted 27 May 2022

Abstract: The gas−liquid two-phase flow behavior in a stirred tank was numerically simulated using Euler−Euler two-fluid model, SST k−ω turbulence model and the multiple reference frame method. The results showed that among all the influencing factors, the rotation speed had the most significant effect on the stirred tank performance, followed by the damping board width. The parameter combination that can produce the most effective stirring was found through orthogonal test and matrix analysis, to be a paddle height of 950 mm, a paddle spacing of 1300 mm, a damping board width of 525 mm and a rotation speed of 123 r/min. Under this condition, the mixing time decreased from 31.620 to 25.845 s when the gas holdup and relative power consumption was basically unchanged.

Key words: horizontal stirred tank; Euler−Euler model; parameter optimization; orthogonal test; matrix analysis

1 Introduction

Environmental pollution from sulfur dioxide (SO_2) flue gas has limited the development of zinc hydrometallurgy based on a roasting−leaching−electrodeposition process. The emergence of zinc metallurgy technology based on oxygen-rich and oxygen-pressurized direct leaching has been timely. This process converts sulfur in a zinc sulfide concentrate into elemental sulfur for convenient storage and transport, which prevents SO_2 flue gas pollution and is thus considered a green smelting process. This process has considerable potential because of the significant advantages of a short reaction time, low oxygen consumption, high thermal efficiency and compact equipment, among others [1−4].

The leaching efficiency of the zinc sulfide concentrate and the energy consumption of the process depend strongly on the gas−liquid flow in the stirred tank. Several factors affect this flow, including the paddle rotation speed, paddle shape, distance between paddles, paddle height (which corresponds to the distance between the paddle and the bottom of the stirred tank), oxygen flow rate and damping board width. These factors interact with each other. To improve the leaching efficiency of the zinc sulfide concentrate and reduce energy consumption, systematic studies need to be performed to determine the ways in which these factors impact the gas−liquid flow in the stirred tank and to determine the optimal structural and operating parameters for the process.

With the improvement of numerical methods in fluids, computational fluid mechanics have been extensively used over the past few years to study gas−liquid flow in stirred tanks [5−11]. KARADIMOU et al [12], SHI and RDLAND [13,14] and MARION et al [15] numerically simulated the flow field of the stirred tank based on CFD technologies. BAO et al [16], OCHIENG

Corresponding author: Hong-jie YAN, Tel: +86-731-88879863, E-mail: s-rfy@csu.edu.cn
DOI: 10.1016/S1003-6326(23)66159-X

et al [17] and ZHAO et al [18] investigated the influence of intermig impeller combined with experimental measurements. The effects of various influencing factors on the flow behavior in a stirred tank, such as impeller type, stirring speed, paddle spacing and blade diameter, were analyzed through range analysis and variance analysis [19−22]. In summary, many interacting factors may affect gas−liquid flow in a stirred tank. These interactions are not adequately considered in current studies, which are mainly focused on the effects of individual factors.

Therefore, the synthetic actions of factors on gas−liquid flow in a stirred tank are explored in this study. These factors include the paddle height, paddle spacing, damping board width and rotation speed. A matrix analysis is used to perform a multi-objective optimization of the stirred tank parameters, thereby optimizing the flow field in the stirred tank, increasing the leaching efficiency and reducing the energy consumption.

2 Physical and mathematical models

2.1 Physical model

Seven compartments of the horizontal stirred tank have similar structures. To simplify the calculations, the middle compartment is simulated in this study using the structure shown in Fig. 1.

Each sidewall of the stirred tank is provided with one damping board. A double-layer stirring paddle is used, with a 45° axial-flow upper paddle with four vanes and a radial-flow lower paddle with six straight vanes. Oxygen is supplied to the stirred tank via an inlet at the bottom. The height of the liquid level after ventilation is taken as the model height. Multiple reference frames are employed in the model: the region in which the paddle is located is defined within a moving reference frame, and a stationary reference frame is used for other areas.

2.2 Mathematical model

Gas−liquid flow predominates the stirred tank interior. The following assumptions are made to simplify the calculations.

(1) The flow process is stable and continuous, and it is regarded as a steady flow process.

(2) The middle compartment contains an overflow port. As the liquid level generally remains constant, the flow is treated as steady.

(3) As the temperature fluctuations (approx. 15 °C) in a compartment are relatively small, the effect of the temperature on the gas−liquid flow is neglected.

The gas−liquid flow in the stirred tank is described using the Euler−Euler two-fluid model. The continuity equation is

$$\nabla\cdot(\alpha_i\rho_i\boldsymbol{u}_i)=0 \tag{1}$$

where ρ_i denotes the phase density for phase i, α_i denotes the phase fraction, and $\boldsymbol{u}_i$ denotes the phase velocity for phase i.

The gas−liquid momentum equation is

$$\nabla\cdot(\alpha_i\rho_i\boldsymbol{u}_i\otimes\boldsymbol{u}_i)=-\alpha_i\nabla p+\nabla\cdot\bar{\bar{\boldsymbol{\tau}}}_i+\alpha_i\rho_i\boldsymbol{g}+(\boldsymbol{F}_i^{\mathrm{Drag}}+\boldsymbol{F}_i^{\mathrm{VM}}+\boldsymbol{F}_i^{\mathrm{Lift}}+\boldsymbol{F}_i^{\mathrm{Disp}}) \tag{2}$$

where ∇p is the gradient of pressure; $\nabla\bar{\bar{\boldsymbol{\tau}}}_i$ is the stress−strain tensor for phase i; $\boldsymbol{g}$ is the acceleration due to gravity; $\boldsymbol{F}_i^{\mathrm{Drag}}$ denotes the drag force, which is described by the model proposed by TOMIYAMA et al [23]. Due to the large difference between the densities of the gas and liquid phases, the virtual mass force ($\boldsymbol{F}_i^{\mathrm{VM}}$) cannot be ignored, and the coefficient of the virtual mass force (C_{VM}) is set to be 0.5 based on numerical simulation research

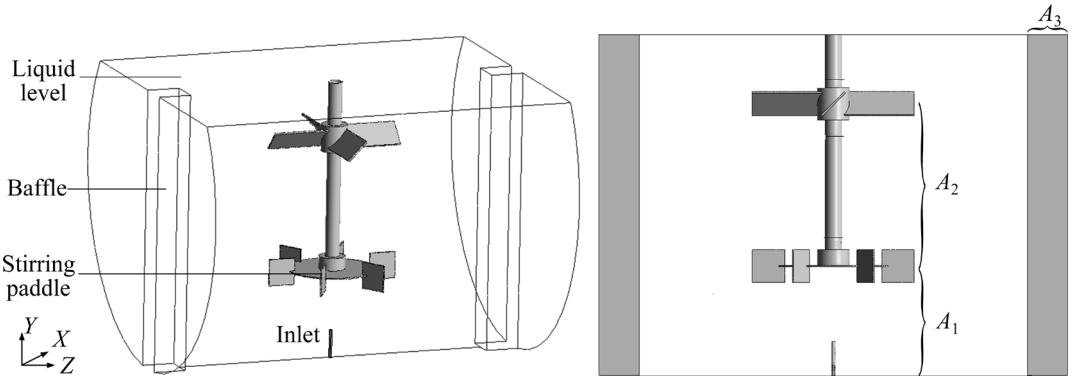

Fig. 1 Schematic of stirred tank (A_1: Paddle height, A_2: Paddle spacing, A_3: Damping board width)

results of MOUGINET and MAGNAUDET [24]. $\boldsymbol{F}_i^{\mathrm{Lift}}$ denotes the lift force and in this study, it is described by the model proposed by TOMIYAMA et al [25]. $\boldsymbol{F}_i^{\mathrm{Disp}}$ represents the turbulent dissipation force and is described by the model proposed by BURNS et al [26].

Since the flow is turbulent at the oxygen inlet (given the Reynolds number Re=13600>2300), the shear stress transport (SST) k–ω turbulence model [27] was used to describe the turbulent process in the stirred tank. In the SST k–ω turbulence model, the transport equations of the turbulence kinetic energy (k) and turbulence frequency (ω) need to be solved. The specific forms of the equations are as follows.

k equation:

$$\nabla\cdot(\alpha_i\rho_i\boldsymbol{u}_i k_i)=\nabla\cdot(\alpha_i\Gamma_k\nabla k_i)+\alpha_i(P_k-\beta'\rho_i k_i\omega_i)+S_i^k \tag{3}$$

ω equation:

$$\nabla\cdot(\alpha_i\rho_i\boldsymbol{u}_i\omega_i)=\nabla\cdot(\alpha_i\Gamma_\omega\nabla\omega)+\alpha_i(C_{\omega P}\frac{\rho_i P_k}{\mu_i^{turb}}-C_{\omega D}\rho_i\omega_i^2)+2\alpha_i(1-F_1)\frac{\rho_i\sigma_{\omega 2}}{\omega_i}\nabla k_i\nabla\omega_i+S_i^\omega \tag{4}$$

where β' is a constant; the density ρ_i and the velocity vector $\boldsymbol{u}_i$ can be treated as known quantities; P_k is a turbulence-induced term; Γ_k and Γ_ω are the diffusion coefficients for k and ω, respectively; F_1 is the mixed function; $C_{\omega P}$, $C_{\omega D}$ and $\sigma_{\omega 2}$ are constants; μ_i^{turb} is the turbulent viscosity; S_i^k and S_i^ω are user-defined source terms.

μ_i^{turb} can be computed by k and ω as follows:

$$\mu_i^{\mathrm{turb}}=\frac{\rho k}{\omega}\frac{1}{\max[\frac{1}{\alpha^*},\frac{\Omega F_2}{a_1\omega}]} \tag{5}$$

where α^* is the low Reynolds number correction coefficient to reduce the viscosity of turbulent vortexes; Ω is the constant term of the shear tensor; a_1 is the empirical constant, and F_2 is the mixing function. In this work, FLUENT method [28] is used to solve the above control equation and SIMPLE [29] algorithm is adopted. The detailed model validation can refer to a previous work [30] using the same physical and mathematical models. The resulting computational time was about 24 h per working condition using a 20 core Intel i7 3.2 GHz CPU.

2.3 Definition of physical properties

The liquid phase in the stirred tank is a zinc sulfate solution, and the gas phase is oxygen at 350 kPa. The physical properties of these two phases are given in Table 1.

Table 1 Physical properties of simulation

Variable	Value
Density of zinc sulfate solution/(kg·m^{-3})	1.35×10^3
Viscosity of zinc sulfate solution/(Pa·s)	0.01
Density of high-pressure oxygen/(kg·m^{-3})	4.89
Viscosity of high-pressure oxygen/(Pa·s)	2.5×10^{-5}
Flow rate at oxygen inlet/(m·s^{-1})	17.14
Bubble diameter/m	0.004

Based on the on-site conditions and flow characteristics, the corresponding boundary conditions are set for the control (Eqs. (1) and (2)). The specific definitions are as follows.

(1) Inlet boundary: Velocity inlet boundary.

(2) Outlet boundary: Degassing boundary. The degassing boundary is used to simulate a free surface, and the gas phase can escape through the boundary.

(3) Wall boundary: The solid wall surface in the tank is set to be in no-slip boundary conditions.

2.4 Grid independency study

Due to the complex combined structure of stirred tank, the structured grid cannot meet the requirements. Therefore, the structured grid and the unstructured grid are combined to divide the computing domain into grid blocks, as shown in Fig. 2.

As shown in Fig. 2, two red-framed regions

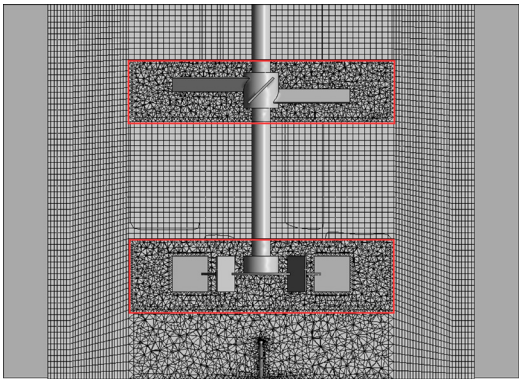

Fig. 2 Schematic diagram of stirred tank grid division

represent the rotation region, while the other regions are stationary regions. The position of the red box is set as the interface. The mesh-independent analysis was carried out for the model of horizontal stirred tank. The above mesh-generation scheme was adopted to divide the stirring models with 8×10^5, 1.2×10^6, 1.6×10^6 and 2×10^6 meshes, respectively. The results of the average gas holdup in the tank were 0.798%, 0.895%, 0.910% and 0.904%, respectively. When the number of grids is 8×10^5, the gas holdup is significantly different from that of 2×10^6, and the relative error is 11.73%. When the number of grids is 1.2×10^6 and 1.6×10^6, the simulation results are close to that of 2×10^6, and the relative errors are 1.01% and 0.66%, respectively. In consideration of the computational amount, the partitioning conditions under the number of 1.2×10^6 grids are adopted in the subsequent studies.

3 Orthogonal test scheme design and numerical simulation results

The oxygen flow in the stirred tank depends on the process conditions and cannot be arbitrarily changed. The four parameters that are optimized in this study are the paddle height, paddle spacing, damping board width and rotation speed, based on the structure and operating conditions of the stirred tank at the respective company, including maintaining the overall structural size and oxygen flow conditions of the stirred tank.

3.1 Orthogonal test design

The following parameter values are used for stirred tank operation in this study: paddle height of 950 mm, paddle spacing of 1300 mm, damping board width of 525 mm, and rotation speed of 123 r/min.

The gas−liquid flow is numerically simulated for the 16 operating conditions in Table 2 to determine the velocity distribution in the gas and liquid phases and the concentration distribution in the gas phase in the stirred tank.

Table 2 Orthogonal test scheme $L_{16}(4^4)$ for optimization of stirred tank parameters

Test No.	Paddle height, A_1/mm	Paddle spacing, A_2/mm	Damping board width, A_3/mm	Rotation speed, A_4/(r·min^{-1})
1	700 (1)	1150 (1)	0 (1)	63 (1)
2	700	1300 (2)	175 (2)	83 (2)
3	700	1450 (3)	350 (3)	103 (3)
4	700	1600 (4)	525 (4)	123 (4)
5	825 (2)	1150	175	123
6	825	1300	0	103
7	825	1450	525	83
8	825	1600	350	63
9	950 (3)	1150	350	83
10	950	1300	525	63
11	950	1450	0	123
12	950	1600	175	103
13	1075 (4)	1150	525	103
14	1075	1300	350	123
15	1075	1450	175	63
16	1075	1600	0	83

The level number of the influencing factor is shown in brackets.

3.2 Evaluation indicators

A uniform oxygen distribution enhances gas−liquid mixing, which promotes the leaching reaction and decreases the time required to mix new pulp into the liquid phase in the stirred tank. The stirred tank space is thus more fully utilized for the pulp leaching reaction, which increases the leaching rate. The mechanical stirring capacity can be affected by the development of “gas cavities” behind the stirring paddle when gas is introduced into the stirred tank. The resulting reduction in the stirring power to below that of a pure liquid phase [31] and the original conveying capacity of the stirring paddle deteriorates gas−liquid dispersion and mixing. Thus, three indicators are used in this study to synergistically evaluate the leaching efficiency and energy consumption of the stirred tank, i.e., the mean gas holdup, mixing time and relative power consumption.

(1) Mean gas holdup

The mean gas holdup indirectly characterizes the uniformity of the gas−phase distribution in the stirred tank and is calculated as a volume-weighted average of the gas holdup in each mesh as follows:

$$\varepsilon=\frac{1}{V}\sum_{i=1}^{N'}a_iV_i \tag{6}$$

where a_i represents the gas holdup of mesh i; V_i

denotes the volume of mesh i; V denotes the total volume of the fluid domain; N' denotes the number of meshes.

(2) Mixing time

The mixing time is an important indicator of the fluid mixing rate in the stirred tank. The mixing time is determined by injecting a tracer with the same physical property parameters as the ore pulp into the overflow port and using the results in conjunction with the following composition equation:

$$\frac{\partial}{\partial t}(\rho Y_i)+\nabla\cdot(\rho \boldsymbol{v} Y_i)=-\nabla\cdot\boldsymbol{J}_i \tag{7}$$

$$\boldsymbol{J}_i=-(\rho D_{i,k}+\frac{\mu_i}{Sc_i})\nabla Y_i \tag{8}$$

where Y_i represents the mass of component i; $\boldsymbol{J}_i$ is the mass diffusion flux relative to the mean velocity; $D_{i,k}$ denotes the diffusion coefficient of component i in component k; and Sc_i is the Schmidt number, which is valued at 0.7 in this study.

Overall monitoring [32] is used to determine the mixing time in this study. The mixing time corresponds to the time at which the fluid volume V_{mix} reaches a prescribed mixing volume fraction M_V (M_V=1) when the tracer concentration is generally equal to the final equilibrium concentration (within ±5% deviation). The mixing volume fraction is calculated by the following equation:

$$M_V=\frac{V_{\text{mix}}}{V_T} \tag{9}$$

where V_T represents the volume of the total fluid domain in the stirred tank. As M_V increases gradually over time, the time needed to reach M_V=1 is the mixing time.

(3) Relative power consumption

The relative power consumption characterizes the degree of reduction in the conveying capacity of the stirring paddle, namely, the ratio of the power consumption after ventilation to that before ventilation. The power consumption of the stirring paddle is calculated using the following equation:

$$P=2\pi NM \tag{10}$$

where n represents the stirring paddle rotation speed, r/s, and m denotes the stirring paddle torque, N·m, which is obtained from a numerical simulation.

3.3 Numerical simulation results of orthogonal test

A total of 16 sets of operating conditions were numerically simulated based on the orthogonal test scheme $L_{16}(4^4)$ given in Table 3. Table 3 shows the mean gas holdup, mixing time and relative power consumption calculated under different operating conditions.

Table 4 presents the results of a range analysis of the data in Table 3.

Table 3 Orthogonal test scheme and corresponding numerical simulation results

Test No.	Level of A_1	Level of A_2	Level of A_3	Level of A_4	Mean gas holdup/%	Relative power consumption	Mixing time/s
1	1	1	1	1	0.9709	0.8596	47.46
2	1	2	2	2	0.9065	0.9785	34.38
3	1	3	3	3	0.8279	0.9621	35.77
4	1	4	4	4	0.8995	0.9856	26.45
5	2	1	2	4	0.7936	0.9893	28.16
6	2	2	1	3	0.8283	0.9495	31.27
7	2	3	4	2	0.9402	0.9640	36.725
8	2	4	3	1	0.9772	0.9213	57.415
9	3	1	3	2	0.8726	0.9394	32.61
10	3	2	4	1	1.0095	0.9610	41.11
11	3	3	1	4	0.8962	0.9911	23.325
12	3	4	2	3	0.8795	0.9107	36.72
13	4	1	4	3	0.9121	0.9867	25.7
14	4	2	3	4	0.8431	0.9732	23.755
15	4	3	2	1	0.9327	0.9046	52.595
16	4	4	1	2	0.9094	0.9661	35.275

Table 4 Range analysis of numerical simulation results

Test evaluation indicator	Variable	Influencing factor			
		A_1	A_2	A_3	A_4
Mean gas holdup, G_1	$k_{1,i,1}$	0.9042	0.9012	0.8873	0.9012
	$k_{1,i,2}$	0.8848	0.8969	0.8781	0.9072
	$k_{1,i,3}$	0.9145	0.8993	0.8802	0.8620
	$k_{1,i,4}$	0.8993	0.9164	0.9403	0.8581
	$s_{1,i}$	0.0296	0.0291	0.0623	0.1145
Relative power consumption, G_2	$k_{2,i,1}$	0.9465	0.9438	0.9416	0.9116
	$k_{2,i,2}$	0.9560	0.9656	0.9458	0.9620
	$k_{2,i,3}$	0.9506	0.9555	0.9490	0.9523
	$k_{2,i,4}$	0.9577	0.9459	0.9743	0.9848
	$s_{2,i}$	0.0112	0.0218	0.0328	0.0732
Mixing time, G_3	$k_{3,i,1}$	36.0150	33.4825	34.3325	49.6450
	$k_{3,i,2}$	38.3925	32.62875	37.96375	34.7475
	$k_{3,i,3}$	33.4413	37.1038	37.3875	32.3650
	$k_{3,i,4}$	34.3313	38.9650	32.4963	25.4225
	$s_{3,i}$	4.9513	6.3363	5.4675	24.2225

The term $k_{h,i,j}$ represents the arithmetic mean of the test evaluation indicator G_h at level j of the influencing factor A_i. The maximum difference in $k_{h,i,j}$ is denoted by $s_{h,i}$:

$$s_{h,i} = \max(k_{h,i,j}) - \min(k_{h,i,j}) \tag{11}$$

where h(=1, 2 and 3) denotes the three test evaluation indicators, i.e., the mean gas holdup, relative power consumption and mixing time, respectively; i(=1, 2, 3 and 4) denotes the four influencing factors, i.e., the paddle height (A_1), paddle spacing (A_2), damping board width (A_3) and rotation speed (A_4), respectively; j(=1, 2, 3 and 4) corresponds to the four levels for each factor.

4 Use of matrix analysis for multi-objective optimization

4.1 Matrix analysis

A matrix analysis of the data in the range analysis table presented above was used to perform a multifactor and multi-objective optimization for the four influencing factors and three test evaluation indicators for the stirred tank.

(1) Layer matrix of test evaluation indicators

By assuming n test evaluation indicators and l influencing factors with m levels each, the layer matrix M_h for the h-th test evaluation indicator is given as follows:

$$\boldsymbol{M}_h = \begin{bmatrix} K_{h,1,1} & 0 & 0 & \cdots & 0 \\ K_{h,1,2} & 0 & 0 & \cdots & 0 \\ \vdots & \vdots & \vdots & \vdots & \vdots \\ K_{h,1,m} & 0 & 0 & \cdots & 0 \\ 0 & K_{h,2,1} & 0 & \cdots & 0 \\ 0 & K_{h,2,2} & 0 & \cdots & 0 \\ \vdots & \vdots & \vdots & \vdots & \vdots \\ 0 & K_{h,2,m} & 0 & \cdots & 0 \\ \vdots & \vdots & \vdots & \vdots & \vdots \\ 0 & 0 & 0 & \cdots & K_{h,l,1} \\ 0 & 0 & 0 & \cdots & K_{h,l,2} \\ \vdots & \vdots & \vdots & \vdots & \vdots \\ 0 & 0 & 0 & \cdots & K_{h,l,m} \end{bmatrix} \tag{12}$$

If a large evaluation indicator produces a more efficient result, then $K_{h,i,j}$ is set equal to $k_{h,i,j}$; if a small evaluation indicator produces a more efficient result, then $K_{h,i,j}$ is set equal to $1/k_{h,i,j}$. Increasing the mean gas holdup and decreasing the time to obtain a uniform mixture improves the leaching rate in the stirred tank. Increasing the relative power consumption reduces the energy consumption of the system.

The layer matrix $\boldsymbol{M}_h$ for the test evaluation indicators has $l \cdot m$ dimensions.

(2) Layer matrix of influencing factors

Considering $k_{h,i,j}$ for G_h, the layer matrix $\boldsymbol{T}_h$ of l influencing factors is an l-dimensional diagonal matrix:

$$\boldsymbol{T}_h=\mathrm{diag}\left[T_{h,1},\ T_{h,2},\ \cdots,\ T_{h,l}\right] \tag{13}$$

where $T_{h,i}=1/\sum_{j=1}^{m}K_{h,i,j}$.

(3) Horizontal layer matrix

The range $s_{h,i}$ of A_i for G_h is described by a horizontal layer matrix $\boldsymbol{S}_h$, which is a column vector with l elements:

$$\boldsymbol{S}_h=\left[S_{h,1},\ S_{h,2},\ \cdots,\ S_{h,l}\right]^{\mathrm{T}} \tag{14}$$

where $S_{h,i}=s_{h,i}/\sum_{i=1}^{l}s_{h,i}$.

(4) Weight matrix of test evaluation indicators

The weight matrix $\boldsymbol{\omega}_h$ (h=1, 2 and 3) of the test evaluation indicators reflects the extent to which different factors affect G_h and is a column vector with $l \cdot m$ elements:

$$\boldsymbol{\omega}_h=\boldsymbol{M}_h\boldsymbol{T}_h\boldsymbol{S}_h=\left[\omega_{h,1,1},\ \omega_{h,1,2},\ \cdots,\ \omega_{h,i,j},\ \cdots,\ \omega_{h,l,m}\right]^{\mathrm{T}}$$

$$\omega_{h,i,j}=K_{h,i,j}T_{h,i}S_{h,i} \tag{15}$$

where $K_{h,i,j}T_{h,i}\left(=K_{h,i,j}/\sum_{j=1}^{m}K_{h,i,j}\right)$ is the ratio of the test evaluation indicator at level j of A_i to the sum of the test evaluation indicators of all levels of A_i; $S_{h,i}$ is the ratio of the range of A_i to the range sum of all the influencing factors. The product $\omega_{h,i,j}$ reflects both the effects of level j of A_i on G_h and the range proportion of A_i. Therefore, the priority and optimization scheme of the influencing factors can be obtained from the weights of the effects at each level of every factor on the test evaluation indicator.

$\boldsymbol{\omega}_h$ (h=1, 2 and 3) indicates the priority of the influencing factors for the three different test evaluation indicators. The optimization scheme for comprehensive performance evaluation is obtained by using the mean of $\boldsymbol{\omega}_h$, that is, $\bar{\boldsymbol{\omega}}=\frac{1}{n}\sum_{h=1}^{n}\boldsymbol{\omega}_h$. Using the data in Table 5 yields the following result:

$$\bar{\boldsymbol{\omega}}=[0.0271,\ 0.0263,\ 0.0280,\ 0.0276,\ 0.0368,\ 0.0375,\ 0.0357,\ 0.0352,\ 0.0548,\ 0.0530,\ 0.0532,\ 0.0574,\ 0.1209,\ 0.1354,\ 0.1366,\ 0.1526]^{\mathrm{T}} \tag{16}$$

In Eq. (16), every four data constitute the weight of the influence of a factor on the comprehensive performance of the stirred tank. The maximum weight is the optimized value of the corresponding factor. Hence, the optimal schemes for the stirred tank are inferred to be A_1=3, A_2=2, A_3=4, and A_4=4; that is, a paddle height of 950 mm, a paddle spacing of 1300 mm, a damping board width of 525 mm, and a rotation speed of 123 r/min.

Figure 3 shows the priority of the influencing factors is $A_4A_3A_2A_1$; that is, the rotation speed has the largest effect (53.46%), followed by the damping board width (21.14%), compared to relatively weak influences for the paddle spacing and height (14.50% and 10.90%, respectively).

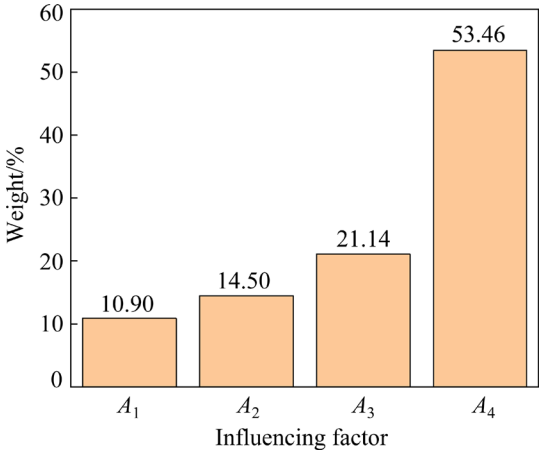

Fig. 3 Weight distribution of influencing factors

4.2 Comparison of numerical simulation results between optimized and base configurations

Table 5 summarizes the above-mentioned optimized and base configurations for the stirred tank. The gas−liquid flow process is numerically simulated under both operating configurations.

(1) Comparison of evaluation indicators

Table 5 Optimized and base operating configurations

Operating configuration	Paddle height/ mm	Paddle spacing/ mm	Damping board width/ mm	Rotation speed/ (r·min^{-1})
Base	846	1410	375	83
Optimized	950	1300	525	123

The comparison of the evaluation indicators for the two configurations shown in Table 6 indicates that all three performance indicators (i.e., the mean gas holdup, relative power consumption and mixing time) of the stirred tank were improved to some extent. Increasing the speed has been reported to decrease the mean gas holdup in a stirred tank [30]. However, this result was not obtained in this study: optimizing the structural parameters of the stirred tank ensured full gas−liquid contact and promoted the chemical reaction in the stirred tank, thus increasing the leaching efficiency. The increased relative power consumption reflected an enhancement of the conveying capacity of the stirring paddle and more efficient fluid stirring in the stirred tank. The reduction in the mixing time reflected faster fluid mixing and higher mixing efficiency.

Table 6 Comparison of base and optimized operating configurations

Operating configuration	Mean gas holdup/%	Relative power consumption	Mixing time/s
Base	0.8833	0.9633	31.620
Optimized	0.8922	0.9879	25.845

(2) Comparison of velocity field for two configurations

To facilitate the observation of the flow field in the tank, a cross-section and longitudinal section of the tank are selected as the characteristic surfaces (as shown in Fig. 4).

Figures 5 and 6 show cloud charts of the velocity distribution in the planes of the upper and lower paddles of the stirred tank under the two

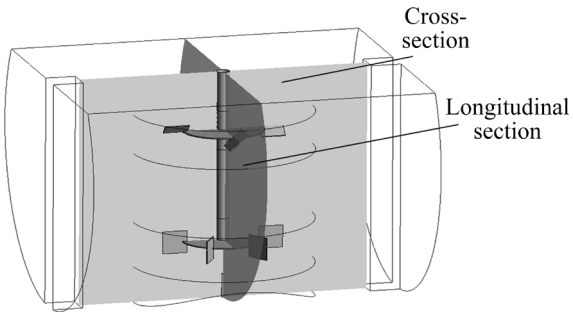

Fig. 4 Schematic diagram of cross-section and longitudinal section of stirred tank

operating configurations. As shown in Fig. 5, with the base configuration (the fluid motion around the impeller), due to the effect of blocking of the damping board, the moving direction of fluids is changed, and the axial velocity and radial velocity are increased. The fluid velocity is faster in the area around the tank wall and damping board, so the mixing effect is good, but in the middle area from the tank wall to the tank center, the fluid velocity is lower, which is not conducive to the gas−liquid mixing.

In the optimized configuration, as shown in Fig. 6, under the optimized configuration, the increased width of the damping board makes the flow from the tank wall to the tank center more disordered, the paddle height and paddle spacing are adjusted to the appropriate position, and the overall stirring intensity in the tank is more uniform, which is conducive to the flow mixing, heat transfer and chemical reaction of the gas−liquid fluid.

Figure 7 shows a cloud chart of the gas holdup distribution for the longitudinal section of the

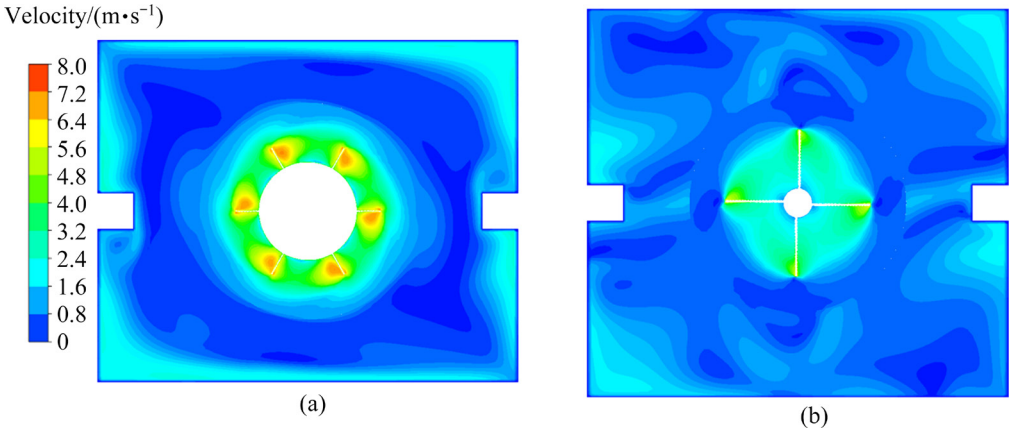

Fig. 5 Velocity distribution in section with upper and lower paddles located in stirred tank with base configuration: (a) Lower paddle; (b) Upper paddle

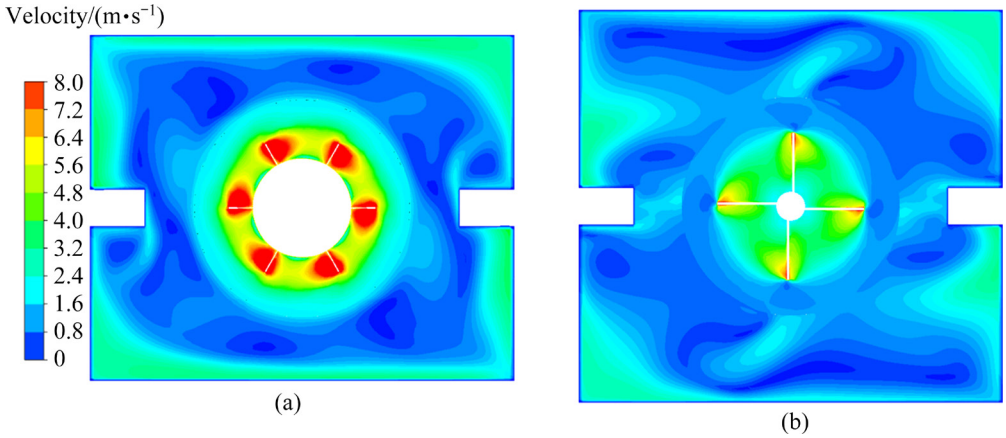

Fig. 6 Velocity distribution in section with upper and lower paddles located in stirred tank with optimized configuration: (a) Lower paddle; (b) Upper paddle

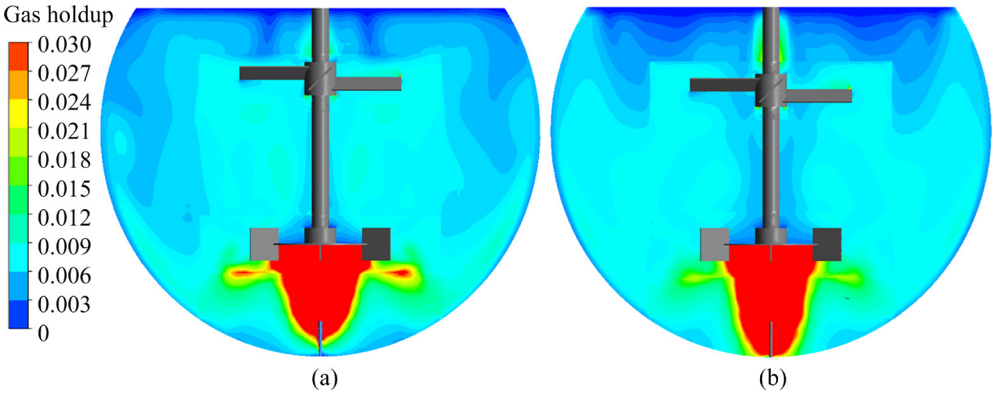

Fig. 7 Cloud chart of gas holdup distribution in longitudinal section of stirred tank: (a) Actual; (b) Optimized

stirred tank. As seen from Fig. 7(a), in the base configuration, under the obstruction of the lower blade disc, the gas phase injected from the bottom oxygen inlet gathers under the blade, and then the gas phase moves around with the liquid phase and rises along the wall of the tank into the circulation area between the two blades. Overall, the gas phase distribution is poor. The gas phase is mainly concentrated under the lower blade and the gas holdup is low in the area between the two blades. For the optimized configuration, increasing the paddle height enables the full development of the gas phase at the bottom of stirred tank. A larger gas-phase volume moves between the two paddle layers to increase the uniformity of the gas-phase distribution, which in turn increases the gas−liquid contact area and the leaching reaction efficiency.

5 Conclusions

(1) The matrix analysis output was used to rank the factors in terms of their effect on the overall stirred tank performance in ascending order as follows: the rotation speed, damping board width, paddle spacing and paddle height.

(2) The results showed that using this optimized configuration (a paddle height of 950 mm, a paddle spacing of 1300 mm, a damping board width of 525 mm and a rotation speed of 123 r/min), improved the mean gas holdup and the relative power consumption of the stirred tank, and reduced the mixing time from 31.620 of the base configuration to 25.845 s.

(3) Using the optimized configuration increased the turbulence of the flow in an intermediate region between the wall and the center of the stirred tank. The higher overall flow rate facilitated gas−liquid mixing. The alleviation of gas-phase enrichment under the paddle resulted in the gas phase being more evenly distributed and therefore more efficient stirring than for the base configuration.

Acknowledgments

The computational resource at the High-Performance Computing Center of Central South University is gratefully acknowledged.

References

[1] ZHANG Jin-xia, ZOU Xuan, NIU Fu-sheng. Leaching behavior and leaching kinetics of zinc from zinc-bearing dust [J]. The Chinese Journal of Nonferrous Metals, 2018, 28(8): 1688−1696. (in Chinese)

[2] NIMA S, JAVAD M, MEHDI O. Kinetics of zinc sulfide concentrate direct leaching in pilot plant scale and development of semi-empirical model [J]. Transactions of Nonferrous Metals Society of China, 2017, 27(10): 2272−2281.

[3] XU Zhi-feng, JIANG Qing-zheng, WANG Cheng-yan. Atmospheric oxygen-rich direct leaching behavior of zinc sulphide concentrate [J]. Transactions of Nonferrous Metals Society of China, 2013, 23(12): 3770−3787.

[4] JIA Li-pan, HUANG Jiang-jiang, MA Ze-long, LIU Xu-heng, CHEN Xing-yu, LI Jiang-tao, HE Li-hua, ZHAO Zhong-wei. Research and development trends of hydrometallurgy: An overview based on Hydrometallurgy literature from 1975 to 2019 [J]. Transactions of Nonferrous Metals Society of China, 2020, 30(11): 3147−3160.

[5] MARKATOS N C. Computer simulation of turbulent fluid flow in chemical reactors [J]. Advances in Engineering Software, 1983, 5(1): 32−38.

[6] SPALDING D B. Numerical computation of multi-phase fluid flow and heat transfer [J]. Recent Advances in Numerical Methods in Fluids, 1980, 1: 139−167.

[7] MARKATOS N C. Modelling of two-phase transient flow and combustion of granular propellants [J]. International Journal of Multiphase Flow, 1986, 12(6): 913−933.

[8] MARKATOS N C. Computational fluid flow capabilities and software [J]. Ironmaking and Steelmaking, 1989, 16(4): 266−273

[9] CAO Xiao-chang, ZHANG Ting-an, ZHAO Qiu-yue. Computational simulation of fluid dynamics in a tubular stirred reactor [J]. Transactions of Nonferrous Metals Society of China, 2009, 19(2): 489−495.

[10] YAN Xiao-sheng, SHAO Hong-gen, LI Qiang. Optimum design of agitator used in acetamiprid crystallizing kettle by using CFD [J]. Chemical and Pharmaceutical Engineering, 2014, 35(2): 44−46, 57. (in Chinese)

[11] XI Chao-chao, WEN Guang-hua, LIU Jiang, XU Song, SUN Xing-hong. Simulation on optimization of flow field in KR hot metal desulfurization ladle [J]. Steelmaking, 2016, 32(1): 1−5, 19. (in Chinese)

[12] KARADIMOU D P, PAPADOPOULOS P A, MARKATOS N C. Mathematical modelling and numerical simulation of two-phase gas−liquid flows in stirred-tank reactors [J]. Journal of King Saud University-Science, 2019, 31: 33−41.

[13] SHI Peng-yu, ROLAND R. Bubbly flow in stirred tanks: Euler−Euler/RANS modeling [J]. Chemical Engineering Science, 2018, 190: 419−435.

[14] SHI Peng-yu, ROLAND R. Solid−liquid flow in stirred tanks: Euler−Euler/RANS modeling [J]. Chemical Engineering Science, 2020, 227: 115875.

[15] MARION A G, RODOLPHE S, CATHERINE X, PHILIPPE H, BERTRAND L, PHILIPPE S. CFD analysis of industrial multi-staged stirred vessels [J]. Chemical Engineering and Processing: Process Intensification, 2006, 45(5): 415−427.

[16] BAO Yu-yun, WANG Bing-jie, LIN Ming-li, GAO Zheng-ming. Influence of impeller diameter on local gas dispersion properties in a sparged multi-impeller stirred tank [J]. Chinese Journal of Chemical Engineering, 2015, 23(4): 615−622.

[17] OCHIENG A, ONYANGO M S, KUMAR A, KIRIAMITI K, MUSONGE P. Mixing in a tank stirred by a Rushton turbine at a low clearance [J]. Chemical Engineering and Processing, 2008, 47(5): 842−851.

[18] ZHAO Hong-liang, ZHANG Zi-mu, ZHANG Tian-an, LIU Yan, GU Song-qing, ZHANG Chao. Experimental and CFD studies of solid–liquid slurry tank stirred with an improved Intermig impeller [J]. Transactions of Nonferrous Metals Society of China, 2014, 24(8): 2650−2659.

[19] SHU Lei, YANG Ming-jin, ZHAO Hang, LI Tian-fu, LI Yang, ZOU Xiang, LI Yun-wu. Process optimization in a stirred tank bioreactor based on CFD-Taguchi method: A case study [J]. Journal of Cleaner Production, 2019, 230: 1074−1084.

[20] CHEN Xiang, WU Han-chuan, QIAO Chun, ZHOU Si-zhu, HUANG Tian-cheng. Optimum design for structure of agitation tank based on orthogonal test method and numerical simulation [J]. Machinery Design, 2012(3): 55−57. (in Chinese)

[21] ZHANG Hui-min, LIAO Hui-liang, HU Shou-min, ZHAO Ya-an. Flow field analysis and structure optimization of open turbine type agitator [J]. Journal of Chinese Agricultural Mechanization, 2016, 37(6): 58−63. (in Chinese)

[22] SATJARITANUNA P, REGALBUTOA J R, REGALBUTOB J A, TIPPAYAWONG N, SHIMPALEE S. Mixing optimization with inward flow configuration contra-rotating impeller, baffle-free tank [J]. Alexandria Engineering Journal, 2021, 60(4): 3759−3779.

[23] TOMIYAMA A, KATAOKA I, ZUN I, SAKAGUCHI T. Drag coefficients of single bubbles under normal and micro gravity conditions [J]. JSME International Journal Series B: Fluids and Thermal Engineering, 1998, 41(2): 472−479.

[24] MOUGIN G, MAGNAUDET J. The generalized Kirchhoff equations and their application to the interaction between a rigid body and an arbitrary time-dependent viscous flow [J]. International Journal of Multiphase Flow, 2002, 28(11): 1837−1851.

[25] TOMIYAMA A, TAMAIA H, ZUN I, HOSOKAWA S. Transverse migration of single bubbles in simple shear flows [J]. Chemical Engineering Science, 2002, 57(11): 1849−1858.

[26] BURNS A D, FRANK T, HAMILL I, SHI J M. The Favre averaged drag model for turbulent dispersion in Eulerian multi-phase flows [C]//5th International Conference on Multiphase Flow. Yokohama, Japan: ICMF, 2004: 392−409.

[27] MENTER F R. Two-equation eddy-viscosity turbulence models for engineering applications [J]. AIAA Journal, 1994, 32(8): 1598−1605.

[28] FLUENT A. Ansys fluent theory guide [M]. USA: Ansys Inc., 2011, 15317: 724−746.
[29] PATANKAR S V. Numerical heat transfer and fluid flow [M]. New York: Hemisphere, 1980.
[30] CHEN Zhi-bin, YAN Hong-jie, ZHOU Ping, YANG Ping, DING Jie-hui, LIU Jia, LIU Liu. Parametric study of gas-liquid two-phase flow field in horizontal stirred tank [J]. Transactions of Nonferrous Metals Society of China, 2021, 31(6):1806−1817.
[31] MONTANTE G, PAGLIANTI A, MAGELLI F. Experimental analysis and computational modelling of gas–liquid stirred vessels [J]. Chemical Engineering Research and Design, 2007, 85(5): 647−653.
[32] HOU Zhi-zhong, FENG Lian-fang, LI Yun-ming, XU Guo-jun, WANG Kai. Gas-liquid dispersion and mixing properties of seven types of impellers in agitated vessels [J]. China Synthetic Rubber Industry, 1995(3): 147−150. (in Chinese)

卧式搅拌釜气液流动数值模拟及多目标参数优化

刘 柳[1]，陈志彬[1]，闫红杰[1]，张登凯[2]，周 萍[1]

1. 中南大学 能源科学与工程学院，长沙 410083；
2. 深圳市中金岭南有色金属股份有限公司 丹霞冶炼厂，韶关 512325

摘 要：采用双欧拉模型、SST k–ω 湍流模型和多重参考系法对搅拌釜内气液两相流动行为进行数值模拟。结果表明：在所有影响因素中，转速对搅拌釜性能的影响最大，其次是挡板宽度。通过正交试验和矩阵分析，发现最优工况为桨叶离底高度 950 mm、桨叶间距 1300 mm、挡板宽度 525 mm 和转速 123 r/min。在优化工况下，保证气含率和相对功耗基本不变时，混匀时间从 31.620 s 缩短至 25.845 s。

关键词：卧式搅拌釜；双欧拉模型；参数优化；正交试验；矩阵分析

(Edited by Bing YANG)